T. RZYCHOŃ*, B. ADAMCZYK-CIEŚLAK**

MICROSTRUCTURE AND CREEP RESISTANCE OF Mg-Al-Ca-Sr ALLOYS

MIKROSTRUKTURA I ODPORNOŚĆ NA PEŁZANIE STOPÓW MAGNEZU Mg-Al-Ca-Sr

Microstructure and creep properties of cast Mg-Al-Ca-Sr alloys have been investigated. The microstructure was characterized using light microscopy, scanning and transmission electron microscopy. Phase identification was made by EBSD technique and by SAED analysis. The measurement of volume fraction of intermetallic phases was performed using quantitative metallography. Creep tests were performed at 180°C and at applied stress between 45 and 90 MPa. Microstructure of tested alloys composed of α-Mg grains and intermetallic compounds in the interdendritic regions. It was found that the addition of calcium and strontium improves creep resistance at 180°C.

Keywords: Cast Magnesium Alloys, Mg-Al-Ca-Sr alloys, microstructure, mechanical properties

W artykule przedstawiono wyniki badań mikrostruktury i odporności na pełzanie odlewniczych stopów magnezu Mg-Al-Ca-Sr. Mikrostrukturę badano metodami mikroskopii świetlnej, skaningowej i elektronowej transmisyjnej. Identyfikacji faz dokonano metodami EBSD i dyfrakcji elektronów (TEM). Pomiar udziałów objętościowych faz dokonano za pomocą metalografii ilościowej. Badania odporności na pełzanie przeprowadzono w temperaturze 180°C przez 100 h. Mikrostruktura badanych stopów składa się z ziaren roztworu stałego α-Mg i faz międzymetalicznych w przestrzeniach międzydendrytycznych. Stwierdzono, że dodatek wapnia i strontu poprawia odporność na pełzanie w temperaturze 180°C.

1. Introduction

Magnesium alloys due to their low density are suitable materials for application in the automotive and aircraft industries. Magnesium alloys based on the Mg-Al system have been studied extensively for use in vehicles due to the weight savings they provide and also for their excellent castability. Commercial magnesium alloys, such as AZ91, AM50 and AM60 have limited application because of poor creep resistance and poor mechanical properties at elevated temperature of 120°C. The cause of this phenomenon is a low-melting point $Mg_{17}Al_{12}$ phase, which is located at the grain boundaries. Therefore, it is important to reduce the amount of $Mg_{17}Al_{12}$ phase and introduce thermally stable precipitates at grain boundaries as well as in the grain interior by adding proper alloying elements. It is well known that alloys of Mg-Al-Ca systems may provide significant improvement in elevated temperature properties due to reduction of volume fraction of $Mg_{17}Al_{12}$ phase and the formation of Al-Ca and Mg-Ca intermetallic compounds [1-8]. The presence of highly stable Laves phases at grain boundaries and in the interior grains has a positive effect on the creep properties of Mg-Al-Ca alloys [9,10]. In general, three Laves phase are observed at interdendritic regions in Mg-Al-Ca alloys: Al_2Ca phase with C15 crystal structure (cubic, $a_0 = 8.02$ Å), Mg_2Ca phase with C14 crystal structure (hexagonal, $a_0 = 6.24$ Å, $c_0 = 10.15$ Å) and $Al_2(Mg,Ca)$ phase with C36 structure (hexagonal, $a_0 = 5.84$ Å, $c_0 = 18.96$ Å) [3, 4, 9-11]. The C15 phase is the most advisable intermetallic compound among the Laves compounds that occur in Mg-Al-Ca alloys due to their high structural stability. The Mg_2Ca compound with a hexagonal C14 type structure has a smaller structural stability in comparison to the C15 phase, however, it is much higher than $Mg_{17}Al_{12}$ phase [12,13]. $Al_2(Mg,Ca)$ phase forms directly from the melt during solidification and transforms to Al_2Ca (C15) phase during aging at elevated temperature [13].

Strontium addition to the Mg-Al-Ca alloys improves the solid-solution strength of the α-Mg phase by increasing the Al solute content and causes the formation of the $Mg_{17}Sr_2$ phase [14], which is identified also as $Al_3Mg_{13}Sr$ [15].

Mg-Al-Ca-Sr alloys are primarily used for components produced by high-pressure die casting method [2]. However, after gravity casting these alloys can reach the mechanical properties at ambient temperatures are comparable to those of expensive Mg-RE-Zn-Zn alloys. The most common representative of Mg-RE-Zn-Zn alloys is ZRE1 alloy (Mg-2.5Zn-3.5RE-0.7Zr in wt.%) which is suitable for components operating at temperatures where creep resistance is required for low stressed complicated castings. ZRE1 alloy is normally used in the T5 condition (10-16 hours at 170-200°C).

*   SILESIAN UNIVERSITY OF TECHNOLOGY, 40-019 KATOWICE, POLAND
**   WARSAW UNIVERSITY OF TECHNOLOGY, 00-661 WARSAW, POLAND

After sand casting and annealing at 200°C for 16 hours, the tensile strength of this alloy is about 140 MPa and yield strength is about 90 MPa [16]. Thus, these alloys can be a cheaper alternative to more expensive magnesium alloys containing zinc and rare earth metals.

2. Experimental procedure

Three magnesium alloys with aluminum, calcium, strontium and manganese were prepared and their compositions, which were analyzed by X-ray fluorescence spectroscopy, are listed in Table 1. Commercially-pure Mg, Al and Mn were used, strontium and calcium were added in the form of Al-10 wt.% Sr and Al-85 wt.% Ca master alloys, respectively. Melting of the alloys was conducted by induction melting in an Al_2O_3 crucible under the protection of an argon atmosphere. The melt was held at 730°C for 3 min then poured into sand moulds.

TABLE 1

The chemical composition of investigated magnesium alloys (wt %)

Alloy	Al	Ca	Sr	Mn	Si	Mg
MgAl5Ca3Sr	5.1	2.96	0.69	0.15	0.25	Balance
MgAl7Ca3Sr	7.3	2.91	0.70	0.12	0.21	Balance
MgAl9Ca1Sr	9.2	0.98	0.91	0.24	0.35	Balance

Microstructural observations of the alloys studied were carried out using scanning electron microscopy (SEM), scanning transmission electron microscopy (STEM) and transmission electron microscopy (TEM). Microanalysis of intermetallic compounds were performed by using energy-dispersive X-ray spectroscopy (EDS). The volume fraction of phases was measured by quantitative metallography. Constant load tensile tests were performed at 180°C and 60 MPa. Creep strain was measured by extensometers which were attached directly to the gauge section of specimens. The length of the specimen was 100 mm, the gage length was 60 mm and the diameter of the reduced section was 6 mm.

3. Results and discussion

3.1. Microstructure

Figure 1 shows SEM micrograph of the MgAl5Ca3Sr alloy. It can be seen that the microstructure of this alloys consists of solid-solution α-Mg and secondary solidification compounds distributing at interdendritic areas. The interdendritic compounds show three morphologies: bulky phase, irregular-shaped eutectic and fine lamellar eutectic. In addition, fine needle-shaped particles inside the α-Mg grains are visible. Energy-dispersive analysis results showed that the irregular eutectic phase contains magnesium, aluminum, calcium (Table 2). It should be noted that the magnesium content in the EDS analysis may be overestimated due to the interaction between the electron beam and magnesium matrix.

Fig. 1. Scanning electron microscope (SEM) images of MgAl5Ca3Sr magnesium alloy, BSE images (a,b), needle-shaped precipitates inside the α-Mg grains, SE image (c)

The content of aluminum dissolved in the magnesium matrix is about 1.4 at.% (Table 2). According to Vegard's rule, if the aluminum content in magnesium solid solution is 1.4 at.%, the lattice parameters of α-Mg should be $a_0 = 3.2044$ Å, $c_0 = 5.2026$ Å [17] (for pure magnesium lattice parameters are $a_0 = 3.209$ Å, $c_0 = 5.211$ Å). Meanwhile, on the basis of X-ray diffraction pattern the measured lattice parameters are $a_0 = 3.2074$ Å, $c_0 = 5.2081$ Å. These results may indicate the dissolution minor amounts of calcium and strontium in the magnesium matrix, because the calcium (197.4 pm) and strontium (215.1 pm) atoms have a larger atomic radius than aluminum atoms (143.2 pm) and their presence in solid solution will increase the unit cell of magnesium. According to the Mg-Ca and Mg-Sr phase equilibrium diagrams, the solubility of calcium and strontium in magnesium is about 0.3 at.% and 0.1 at.%, respectively. Therefore, at such a low solubility in solid solution these alloying elements were not detected during the SEM-EDS microanalysis.

TABLE 2

Average (from 5 points) chemical composition of phases in ACJM53 alloy, at.%, EDS

Phase	Morphology	Mg	Al	Ca	Sr
$\alpha-$Mg	Matrix	98.6±2.0	1.4±0.08	-	-
$(Mg,Al)_2Ca$ - C36	Irregular eutectic	54.2±1.1	30.5±0.9	15.2±0.5	0.1±0.02
$(Mg,Al)_2Ca$ - C14	Fine lamellar eutectic	71.4±2.2	13.6±1.6	12.2±0.7	2.8±0.6
Al_3Mg_{13} (Sr,Ca)	Bulky phase	70.7±3.4	19.9\$±1.9	2.0±0.4	7.4±0.7

In order to identify the existing phases in the alloy selected area diffraction analysis (SAED) was performed. The irregular-shaped phase was identified as $(Mg,Al)_2Ca$ phase with C36 crystal structure (hexagonal, $a_0 = 5.83$ Å, $c_0 = 18.897$ Å) (Fig. 2). A diffraction pattern corresponding to the fine lamellar compound is shown in Fig. 3. The pattern can be indexed to the [-45-12] zone axis of the C14 phase (Mg_2Ca) with hexagonal crystal structure ($a_0 = 6.238$ Å, $c_0 = 10.146$ Å).
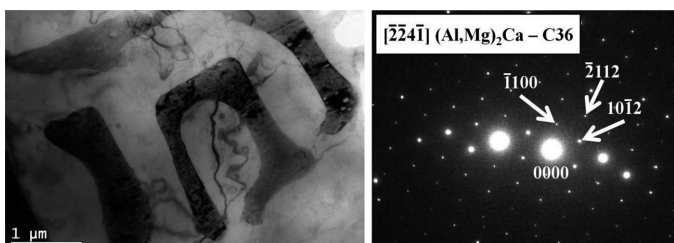

Fig. 2. TEM bright field image and SAED pattern of the $(Al,Mg)_2Ca$ (C36) phase, [-2-24-1] zone axis
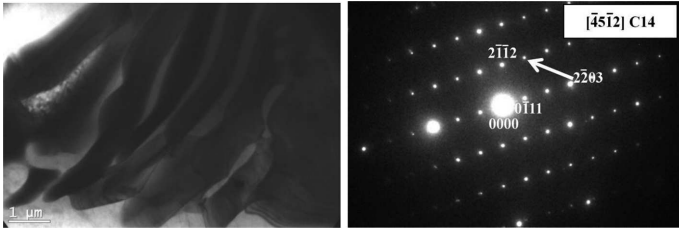
Fig. 3. TEM bright field image and SAED pattern of the Mg_2Ca (C14) phase, [-45-12] zone axis

The bulky phase containing Mg, Al and Sr was also observed in Mg-Al-Sr alloys and tentatively designated as stoichiometry $Al_3Mg_{13}Sr$ [15]. In previous investigations using the Rietveld method [18], we reported that the bulky phase in AJ63 magnesium alloy has a crystal structure which is isomorphous with crystal structure of $Mg_{12}Nd$ compound (tetragonal *I4/mmm* crystal structure, $a_0 = 10.31$ Å, $c_0 = 5.93$ Å). SAED pattern obtained from this phase confirms the presence of massive phase having a tetragonal crystal structure isomorphous to $Mg_{12}Nd$ phase (Fig. 4). However, A. Suzuki et. al. [14] identified the $Al_3Mg_{13}Sr$ compound using transmission electron microscopy as the $Mg_{17}Sr_2$ (hexagonal *hP38* crystal structure) phase with solubility of aluminum. Therefore, the identification of the bulky phase will be subject of further studies. The needle-shaped precipitates within α-Mg grains was identified as Al_2Ca phase with C15 crystal structure (cubic, $a_{0=} 8.02$ Å) (Fig. 5).
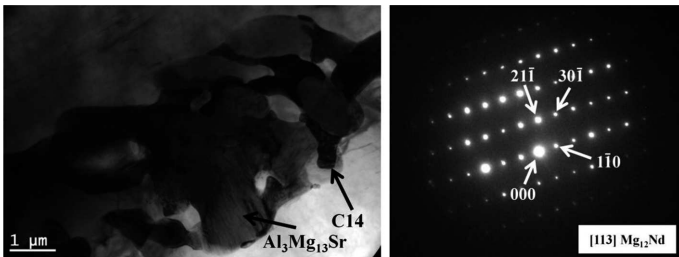

Fig. 4. TEM bright field image and SAED pattern of the $Al_3Mg_{13}Sr$ phase, which is isomorphous with $Mg_{12}Nd$ compound, [113] zone axis
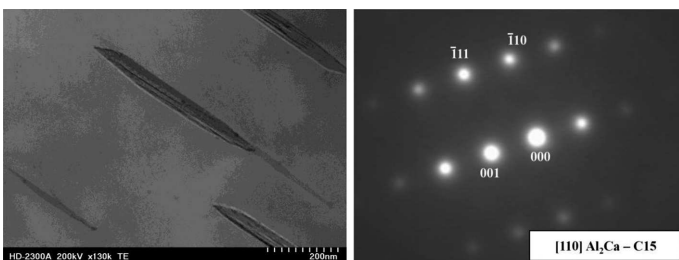

Fig. 5. STEM bright field image and SAED pattern (STEM electron nanodiffraction technique) of the needle-shaped Al_2Ca (C15) phase, [110] zone axis

Microstructure of MgAl7Ca3Sr alloy is similar to microstructure of MgAl5Ca3Sr alloy (Fig. 6a). The volume fraction of C36, $Al_3Mg_{13}Sr$ and C14 phases is comparable in both alloys, whereas in MgAl7Ca3Sr alloy the volume fraction of C15 phase is slightly lower (Table 3) and the content of aluminum dissolved in the α-Mg solid solution (2.0±0.1 at.%) is higher than in MgAl5Ca3Sr alloy (1.4±0.08 at.%).

Microstructure of MgAl9Ca1Sr alloy is significantly different from the microstructure of the other alloys (Fig. 6b). The $(Mg,Al)_2Ca$-C36 compound is dominant intermetallic phase in the interdendritic regions. The bulky $Al_3Mg_{13}Sr$ phase and fine lamellar Mg_2Ca phase were not observed in this alloy. J. Bai et al. [19] reported that the increase of Al content leads to the formation Al_4Sr phase at grain boundaries and disappearance of the bulky phase in Mg-Al-Ca-Sr alloys. Also in our Al-rich alloy, we found thin lamellar Al_4Sr phase with tetragonal crystal structure ($a_0 = 4.46$ Å, $c_0 = 11.07$ Å) (Fig. 7). Due to the high aluminum and low calcium contents the $Mg_{17}Al_{12}$ phase is observed in the microstructure of MgAl9Ca1Sr (Fig. 8). Moreover, supersaturated α-Mg solid solution areas are visible in the vicinity of interdendritic areas (dark areas in Fig. 6b).

TABLE 3

Volume fraction of intermetallic phases (vol. %)

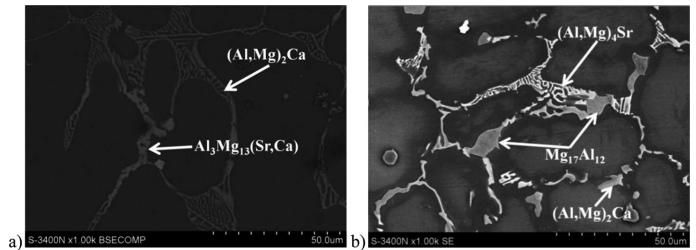| Alloy	$(Mg,Al)_2$ Ca-C36	Al_3Mg_{13} (Sr,Ca)	Al_2Ca -C15	Mg_2Ca -C14	$Mg_{17}Al_{12}$	Al_4Sr
MgAl5 Ca3Sr	5.9	1.2	0.9	0.9	-	-
MgAl7 Ca3Sr	5.8	0.9	0.4	0.8	-	-
MgAl9 Ca1Sr	4.0	-	-	-	0.9	0.8

Fig. 6. Microstructure of as-cast MgAl7Ca3Sr alloy (a) and of MgAl9Ca1Sr alloy (b). In dark areas surrounded the intermetallics compounds the higher content of aluminum was found than in the centre of α-Mg grains
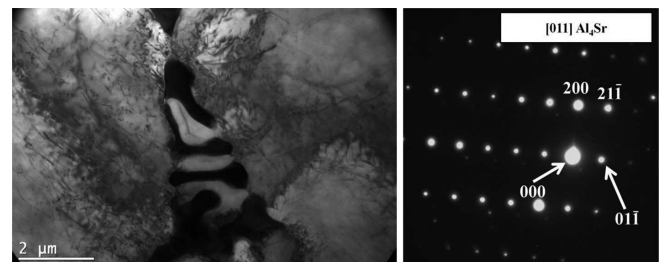

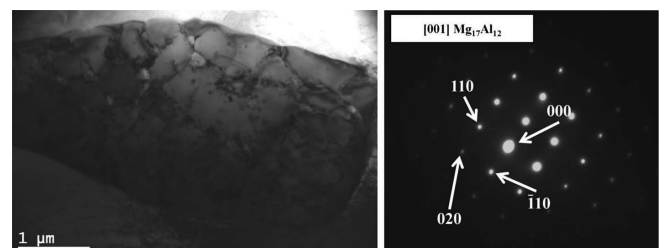Fig. 7. TEM bright field image and SAED pattern of the Al_4Sr phase, [011] zone axis, MgAl9Ca1Sr alloy

Fig. 8. TEM bright field image and SAED pattern of the $Mg_{17}Al_{12}$ phase, [001] zone axis, MgAl9Ca1Sr alloy

332

3.2. Creep properties

The creep tests in the present investigation were carried out at a temperature of 180°C and at applied stress between 45 and 90 MPa. The 100 h creep curves for the Mg-Al-Sr-Ca alloys tested at different stresses and at 180°C are shown in Fig. 9 and 10. From the gradient of the secondary stage in the creep curves, the steady-state creep rate can be calculated and the results are shown in Table 4. Obviously, the steady-state creep rate and creep strain increased with increases in the applied stress.
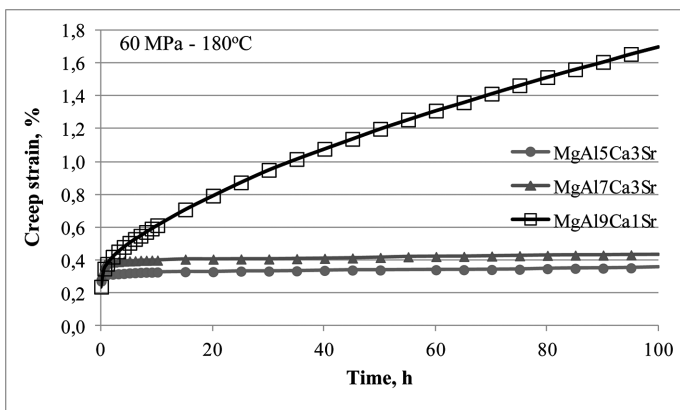

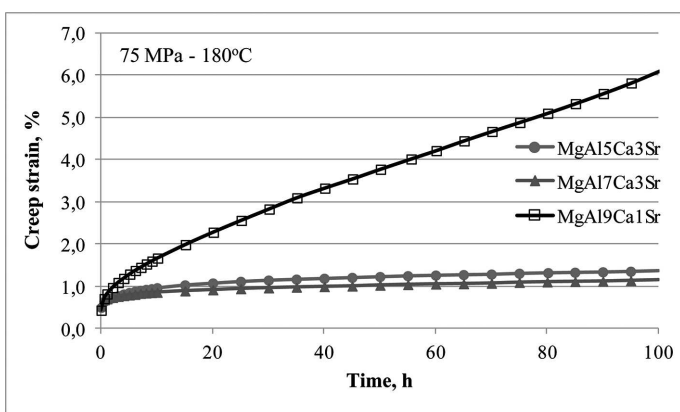Fig. 9. Creep curves of tested alloys at 180°C and at 60 MPa

Fig. 10. Creep curves of tested alloys at 180°C and at 75 MPa

The MgAl9Ca1Sr alloy has good creep resistance at a stress of 45 MPa, whereas above 60 MPa the creep resistance decreases dramatically. The MgAl5Ca3Sr and MgAl7Ca3Sr alloys reach a much better creep resistance up to 75 MPa. The low creep properties of MgAl9Ca1Sr alloy are associated with the presence of low-melting $Mg_{17}Al_{12}$ phase in the microstructure and precipitation of $Mg_{17}Al_{12}$ phase from supersaturated areas of α-Mg matrix (Fig. 11). The $Mg_{17}Al_{12}$ phase cannot act as a barrier to dislocations movement, whereas the precipitation process depletes the matrix of aluminum and thus reduces the effect of solid solution strengthening.

In the Ca-rich alloys the irregular eutectic $(Mg,Al)_2Ca$ (Fig. 12) and bulky $Al_3Mg_{13}(Sr,Ca)$ phases seems to be stable during creep at 180°C and 60 MPa, however microvoids localized in the interdendritic regions were also observed. Moreover, during creep of the MgAl5Ca3Sr and MgAl7Ca3Sr alloys, the precipitation of Al_2Ca phase occurred in the α-Mg

solid solution (Fig. 13). It should be noted that the needle precipitates of Al_2Ca were also visible in as-cast state, but their length did not exceed 0.5 μm, whereas in samples after creep tests, precipitates of the Al_2Ca phase had a length of about 2 μm. Thus, the better creep resistance of MgAl5Ca3Sr and MgAl7Ca3Sr alloys, in comparison to the MgAl9Ca1Sr alloy, is caused by a precipitation process and the presence of stable C36, C14, C15 and $Al_3Mg_{13}Sr$ intermetallic compounds.

TABLE 4

Results of creep tests of the tested alloys

|	Stress, MPa	Temperature, °C	Time of test, h	Initial creep strain ε_p, %	Total creep strain ε, %	Creep rate $\dot{\varepsilon}$, 1/s
MgAl5Ca3Sr	45	180	100	0.15	0.28	$1.1\cdot10^{-10}$
MgAl7Ca3Sr	45	180	100	0.16	0.27	$9.0\cdot10^{-11}$
MgAl9Ca1Sr	45	180	100	0.11	0.92	$8.5\cdot10^{-9}$
MgAl5Ca3Sr	60	180	100	0.31	0.36	$1.0\cdot10^{-9}$
MgAl7Ca3Sr	60	180	100	0.31	0.43	$1.3\cdot10^{-9}$
MgAl9Ca1Sr	60	180	100	0.24	1.7	$3.1\cdot10^{-8}$
MgAl5Ca3Sr	75	180	100	0.50	1.38	$9.9\cdot10^{-9}$
MgAl7Ca3Sr	75	180	100	0.54	1.15	$7.9\cdot10^{-9}$
MgAl9Ca1Sr	75	180	100	0.44	6.1	$1.3\cdot10^{-7}$
MgAl5Ca3Sr	90	180	16	1.37	5.17	$4.9\cdot10^{-7}$
MgAl7Ca3Sr	90	180	31	1.47	6.1	$8.4\cdot10^{-8}$
MgAl9Ca1Sr	90	180	9	1.2	7.2	$1.3\cdot10^{-5}$
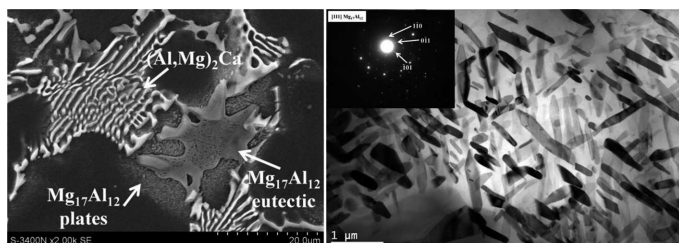
Fig. 11. Microstructure of MgAl9Ca1Sr alloy after creep testing at 180°C and 60 MPa with platelet precipitates of $Mg_{17}Al_{12}$ phase formed in supersaturated areas of α-Mg matrix
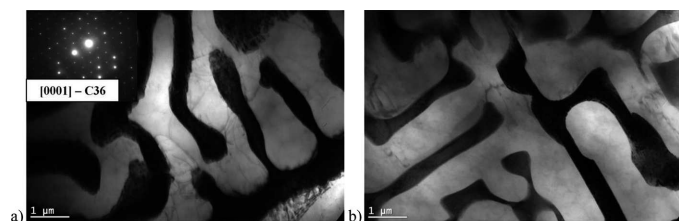

Fig. 12. Microstructure of MgAl5Ca3Sr (a) and MgAl7Ca3Sr (b) alloys after creep testing at 180°C and 60 MPa with the irregular $(Al,Mg)_2Ca$ (C36) phase

It is generally agreed that the creep rate in the secondary stage $\dot{\varepsilon}_s$ is described by a power law equation in the stress σ and temperature T ranges of σ = 20-100 MPa and T = 100-250°C.

$$\dot{\varepsilon}_s = A\sigma^n \exp\left(\frac{-Q_s}{RT}\right) \qquad (1)$$

where A is a constant, n the apparent stress exponent, R the gas constant and Q_s is the apparent activation energy. The n and Q_s parameters can be used to infer the dominant creep mechanisms for a material in specific ranges of stress and temperature [7].
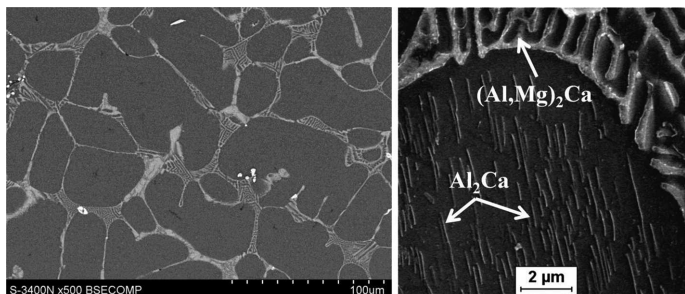

Fig. 13. Microstructure of the MgAl5Ca3Sr magnesium alloy after creep testing at 180°C and 60 MPa

By measuring the slope of the log versus $\log\sigma$ plot and assuming that the data could be described by the Eq. (1), the stress exponents were calculated and results are presented in Fig. 14. The number of data points is not sufficient to evaluate Q_s.
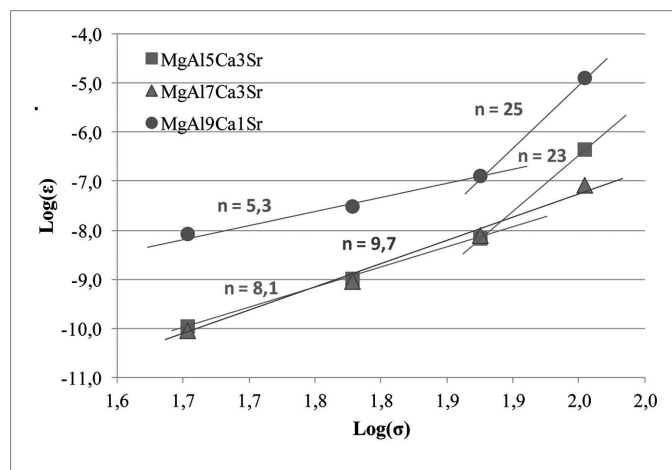

Fig. 14. Plots of creep rates against stress for the tested alloys

As shown in Fig. 14, the creep rates of MgAl9Ca1Sr alloy exhibit two-stage behavior with $n \approx 5$ at low stresses (45-75 MPa) and much higher value of n, which is 25 at higher stresses (above 75 MPa). For most of Mg-Al based alloys, grain boundary sliding has been observed for low-stress creep ($n = 2$), which is accompanied by discontinuous precipitation of $Mg_{17}Al_{12}$ phase from a supersaturated α-Mg matrix. For high-stress creep ($n = 5$), dislocation climb creep is proposed as the dominant mechanism [7,20]. Thus, the creep of MgAl9Ca1Sr alloy at 45-75 MPa stress level seem to be dislocation controlled. Because in the microstructure of this alloy after creep tests at 180°C the discontinuous precipitates of $Mg_{17}Al_{12}$ phase were observed, the contribution to creep by grain boundary sliding cannot be ignored in this alloy. Whereas an abrupt increase of stress exponent of 25 indicate a power-law breakdown.

The MgAl5Ca3Sr alloy exhibits similar behavior during the creep tests, however in this case the value of stress exponent ($n \approx 8$) at low stresses is higher than in MgAl9Ca1Sr

alloy. The increase in n value (at the lower creep rates) for the MgAl5Ca3Sr1 alloy is probably due to the presence of needle-shaped Al_2Ca phase within α-Mg grains [21]. Above 75 MPa the stress exponent increases to 23, which indicates a power-law breakdown.

The MgAl7Ca3Sr alloy does not show two-stage creep regime and the value of n is close to 10. Analysis microstructure of this alloy after creep tests, which will be presented elsewhere, indicates that during the creep of this alloy, the precipitation of Al_2Ca phase within α-Mg grains is observed. Thus, the value of stress exponent in range of 8-10 at low creep rates may indicate the course the precipitation process of needle-shaped Al_2Ca phase during creep at 180°C for Ca-rich Mg-Al-Ca-Sr alloys. Nevertheless, grain boundary sliding or dislocation controlled creep can still make strong contributions to the overall creep strain.

4. Conclusions

The microstructure of MgAl5Ca3Sr and MgAl7Ca3Sr alloys consists of α-Mg matrix, irregular $(Mg,Al)_2Ca$ eutectic phase with C36 the crystal structure, fine lamellar Mg_2Ca (C14) eutectic phase, bulky $Al_3Mg_{13}(Sr,Ca)$ phase and needle-shaped Al_2Ca phase with C15 crystal structure. Microstructure of MgAl9Ca1Sr consists of α-Mg, $(Mg,Al)_2Ca$ - C36, Al_4Sr and $Mg_{17}Al_{12}$ phases. The alloys containing 3 wt% calcium have good creep resistance at temperature of 180°C and stresses in range of 45-75 MPa. The MgAl9Ca1Sr alloy possesses good creep properties only at 45 MPa. Good creep resistance of MgAl5Ca3Sr and MgAl7Ca3Sr alloys is associated with the presence of the stable intermetallic compounds in the interdendritic regions and presence of needle-shaped Al_2Ca phase within α-Mg grains. The presence of $Mg_{17}Al_{12}$ phase in the MgAl9Ca1Sr alloy results in a lower creep resistance at 180°C.

REFERENCES

[1] H.T. S o n, J.S. L e e, C.S. K a n g, J.C. B a e, K. Y o s h i m i, K. M a r u y a m a, Mater. Trans. **49**, 945-951 (2008).

[2] A.A. L u o, B.R. P o w e l l, A.K. S a c h d e v, Intermetallics **24**, 22-29 (2012).

[3] A. S u z u k i, N.D. S a d d o c k, J.W. J o n e s, T.M. P o l - l o c k, Scr. Mater. **51**, 1005-1010 (2004).

[4] J. B a i, Y. S u n, F. X u e, J. Z h o u, Mat. Sci. Eng. A **531**, 130-140 (2012).

[5] Y. T e r a d a, N. I s h i m a t s u, T. S a t o, Mater. Trans. **48**, 2329-2335 (2007).

[6] T. R z y c h o ń, B. A d a m c z y k - C i e ś l a k, A. K i e ł b u s, J. M i z e r a, Materialwiss. Werkstofftech. **43**, 421-427 (2012).

[7] B. P ł o n k a, M. L e c h - G r e g a, K. R e m s a k, P. K o r - c z a k, A. K ł y s z e w s k i, Arch. Metall. Mater. **58**, 127-132 (2013).

334

[8] D. Kuc, E. Hadasik, I. Schindler, P. Kawulok, R. Sliwa, Arch. Metall. Mater. **58**, 151-156 (2013).

[9] S. Amerioun, S.I. Simak, U. Häussermann, Inorg Chem. Mar. **42(5)**, 1467-1474 (2003).

[10] R. Ninomiya, T. Ojiro, K. Kubota, Acta Metall. Mater. **43**, 669-674 (1995).

[11] A.A. Luo, M.P. Balogh, B.R. Powell, Metall. Mater. Trans. A **33A**, 567-574 (2002).

[12] D.W. Zhou, J.S. Liu, P. Peng, L. Chen, Y.J. Hu, Mater. Lett. **62**, 206 (2008).

[13] A. Suzuki, N.D. Saddock, J.W. Jones, T.M. Pollock, Acta Mater. **53**, 2823-2834 (2005).

[14] A. Suzuki, N.D. Saddock, L. Riester, E. Lara-Curzio, J.W. Jones, T.M. Pollock, Metall. Mater. Trans. A **38A**, 420-427 (2007).

[15] E. Baril, P. Labelle, M.O. Pekguleryuz, J. Metals **55**, 34-39 (2003).

[16] T. Rzychoń, J. Szala, A. Kiełbus, Arch. Metall. Mater. **57**, 254-262 (2012).

[17] D. Hardie, R.N. Parkins, Philos. Mag. **4**, 815 (1959).

[18] T. Rzychoń, A. Kiełbus, G. Dercz, Solid State Phenom. **163**, 169-172 (2010).

[19] J. Bai, Y. Sun, F. Xue, S. Xue, J. Qiang, T. Zhu, J Alloy. Compd. **437**, 247-253 (2007).

[20] J. Bai, Y. Sun, S. Xun, F. Xue, T. Zhu, Mater. Sci. Eng. A **419**, 181-188 (2006).

[21] T. Rzychoń, J. Szala, T. Kukiełka, Solid State Phenom. **197**, 137-142 (2013).